L. Back

OFFICE NATIONAL D'ÉTUDES ET DE RECHERCHES AÉROSPATIALES
29, Avenue de la Division Leclerc - 92 CHATILLON France

STUDY OF THE ACCURACY OF GAS FLOW MEASUREMENTS USING THE SONIC THROAT METHOD

TRANSLATION OF

ÉTUDE DE LA PRÉCISION DES MESURES DE DÉBITS GAZEUX PAR LA MÉTHODE DU COL SONIQUE

by ~~par~~ Bernard MASURE

Communication présentée à l'Association Technique Maritime et Aéronautique (A.T.M.A.)
Paris, 6-10 mai 1968

Translated under NAS 7-100
JPL, [redacted]
Pasadena, cal.

OVC P.M

TIRÉ A PART : T.P. n° 572 (1968)

STUDY OF THE ACCURACY OF GAS FLOW MEASUREMENTS USING THE SONIC THROAT METHOD

B. Masure
Research Engineer, National Bureau of Aerospace Research

SUMMARY

The formula leading to a calculation of a gas flow using the sonic throat method is recalled. /1*

This relationship, which is deduced from the monodimensional theory and is applied to the flow of a gas without viscosity and constant specific heat, must be affected by three corrective factors. These three factors are analyzed in the case of air in succession: curvature of the sonic line, viscosity, effect of compressibility.

Some experiments are described which confirm the calculation of the compressibility effect.

INTRODUCTION

Present-day industrial measurements of gas flow do not customarily have great accuracy. An error on the order of 1 to 2% is permissible. The situation is not the same when, for example, we consider the production of the supersonic transport, where the accuracy required in calculating the flow is several thousandths.

The use of a sonic throat, which can be put into operation very simply, /2
seems to be the most practical means of obtaining such accuracy. We shall analyze this method in this article.

The mono-dimensional theory applied to a gas flow without viscosity, to the throat of a flowmeter which has been started, makes it possible to write

*Numbers in the margin indicate pagination in the original foreign text.

the following

$$\bar{q} = \rho_c \cdot a_c \cdot A_c \qquad \text{(c: critical conditions)} \quad (1)$$

If this gas is perfect and has constant specific heat, a simple transformation gives us

$$\bar{q} = \left[\sqrt{\frac{\gamma}{R}} \cdot \frac{\rho_c}{\rho_i} \cdot \frac{a_c}{a_i}\right] \times \frac{P_i A_c}{\sqrt{T_i °K}} \qquad \text{(i:stagnation conditions)} \quad (2)$$

where the term between the brackets is a function of γ and R.

Relationship (2) shows that the measurements of P_i and T_i make it possible to arrive at the flow $\bar{q}$ if the three hypotheses of monodimensional outflow, absence of viscosity, and gas which is perfect in terms of heat are satisfied. In the opposite case, expression (2) must be affected by a corrective factor C_D which we are going to determine in the case of rotating flowmeters having a circular meridian and supplied with dry air, regarded as a real gas.

1. Effect of Curvature of the Sonic Line

1.1. Introduction

The resolution by methods similar to the potential equation for the flow of a gas which is perfect in terms of heat and is irrotational shows that the sonic surface is not planar and that -- due to this fact -- the flow is less than that of monodimensional theory.

In general, these similar methods consist of imposing a law of velocity distribution on the axis of symmetry, in the vicinity of the sonic point and -- by means of a limited expansion of the flow function -- of deducing from this the flow in the vicinity of the axis. The direction of the flow lines can then be deduced and the radius of curvature at the top of these lines can be calculated, which makes it possible to define the local geometry of flow. In a reciprocal manner, a velocity gradient on the axis and a particular flow may be associated with a local geometry, characterized by the ratio $\frac{R_c}{h}$ of the radius of curvature R_c of the meridian to the half-height h of the nozzle.

Unfortunately, the convergence of the series expansion is by no means assured and -- if the solutions obtained may be regarded as being valid in the immediate vicinity of the axis, i.e., for sufficiently large values of R_c/h -- there are very great doubts as to the small values of R_c/h. For example, in reference [1], the flow function $\phi(s,y)$ is expanded up to the 6th order with respect to x and y. /3 The flow obtained then makes it possible to calculate the descending characteristic starting from the sonic point, and makes it possible to substantiate the fact, a posteriori, that along this line the compatability conditions of the Cauchy problem are satisfied. This may be done in a satisfactory manner if $R_c/h \geq 2.4$ in the plane case.

1.2. Plane Case

If we first consider the case of a plane pipe, it is known that the choice of the velocity modulus V and the polar angle θ as independent variables makes it possible -- by using the Molenbrock-Tchapliguine transformation -- to obtain a system of linear, partial differential equations. If, on the other hand, we employ a compressibility law which -- in the vicinity of the critical conditions -- is satisfactorily close to the compressibility law for a perfect gas, we can obtain an exact, analytical solution in the transonic region [2]. A recent numerical experiment [3], with a compressibility law which is more refined than those proposed in [2], then makes it possible to calculate the corrective factor C_{D_k} which may be applied to (2) to take into account this effect of curvature:

$$C_{D_k} = \frac{\text{yield with effect of curvature of the sonic line}}{\text{yield of monodimensional flow}}$$

Cuve A in Figure 1 gives the variations of this coefficient as a function of /4 h/R_c. (h: half-height of the throat; R_c: radius of curvature of the meridian).

However, it should be noted that the exact analytical solution obtained in [2], [3] imposes a certain flow in the region of increased subsonic flow. Consequently, the solution obtained in the region of the throat is only strictly valid if there is agreement between transonic flow obtained from the exact solution

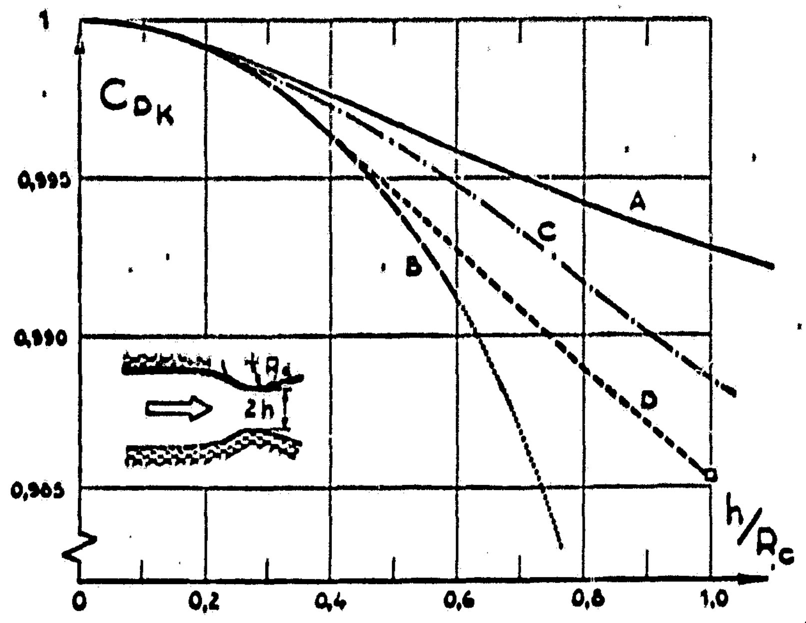

Figure 1. Calculation of the Flow. Effect of the Sonic Line Curvature.
A: Plane case; exact solution.
B: Case of rotation:Hall formula with three terms.
C: Case of rotation: Central line of the probable zone proposed by Stratford.
D: Case of rotation: Curve proposed by the author.

and the subsonic flow which precedes it.

If we assume as a first approximation -- as experiments have indicated -- that the nature of the flow in the sonic region is only slightly changed by the flow in the subsonic region, we may regard the curve A as universal, which is independent of the upstream conditions and which may be applied to the case of <u>plane pipes</u>.

1.3. <u>Case of Rotation</u>

If we now deal with the case of <u>rotating pipes</u>, it is not possible to obtain an exact analytical solution, and at the present time we may/obtain ~~only~~ obtain approximate solutions.

All of the solutions proposed are similar to each other for small curvatures, but great disparity appears among the authors for large curvatures.

In Figure 1, we have shown (curve B) the variation of C_{D_k} as a function of h/R_c obtained from the Hall formula with three terms [4], and applied to the case of rotation. The solution proposed by Hall is in the form of a series with respect to h/R_c, of which only the first three terms are retained. According to [5], this

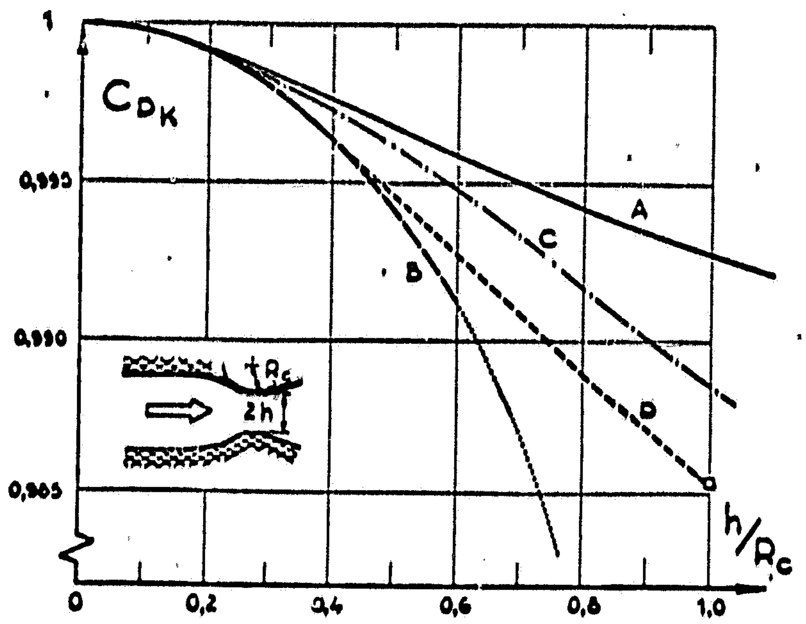

Figure 1. Calculation of the Flow. Effect of the Sonic Line Curvature.
A: Plane case; exact solution.
B: Case of rotation:Hall formula with three terms.
C: Case of rotation: Central line of the probable zone proposed by Stratford.
D: Case of rotation: Curve proposed by the author.

and the subsonic flow which precedes it.

If we assume as a first approximation -- as experiments have indicated -- that the nature of the flow in the sonic region is only slightly changed by the flow in the subsonic region, we may regard the curve A as universal, which is independent of the upstream conditions and which may be applied to the case of series probably diverges for the values of $h/R_c \geq 0.625$. This is the reason why curve B is drawn in a dotted line for $h/R_c \geq 0.6$.

In reference [6], Stratford, in comparing a group of theoretical results with experimental results, suggests a region inside of which the valid values of C_{D_k} must be logically located. This region is limited by an upper curve and a lower curve. We have shown in Figure 1, curve C, the average of these extreme values. Finally, curve D is obtained from the very fragmentary experimental results which are described later.

1.4. Conclusion

We have tried to determine in a rather large region

$$(0 \leqslant h/R_c \leqslant 1)$$

the variations of the coefficient C_{D_k} in the case of rotation.

/5

Due to the great dispersion which occurs for large curvatures, for purposes of accuracy one should avoid designing the flowmeters with these curvatures.

2. Effect of Viscosity [7]

The effect of displacement caused by the boundary layer is characterized by the thickness $\delta^{(1)}$. A reduction in the flow results

$$\frac{\delta q}{q} = -2\frac{\delta_c^{(1)}}{h}.$$

The problem therefore amounts to determining $\delta_c^{(1)}$ at the throat.

We shall confine ourselves to the case of a turbulent boundary layer developing along an athermanous wall ($T_p = T_f$). We are then led to integrate the Karman equation:

$$\frac{d\delta^{(2)}}{dx} + \delta^{(2)}\left[\frac{H+1}{u_e}\frac{du_e}{dx} + \frac{d}{dx}\operatorname{Log}\left(\rho_e u_e Y\right)\right] = \frac{\tau_p}{\rho_e u_e^2} = \frac{C_f}{2} \tag{3}$$

where $\delta^{(2)}$ represents the momentum thickness.

This integration must be preceded by a hypothesis with respect to the quantities H and C_f.

For H, the calculations performed by R. Michel [8] yield the following expression in the athermanous case:

$$\frac{\delta^{(1)}}{\delta^{(2)}} = H = 1{,}4 + 0{,}4\, M_e^2$$

On the other hand, the concept of the reference temperature proposed by Eckert makes it possible to write the following:

$$C_f = \frac{0{,}0172}{\left(\frac{\rho_e u_e \zeta^{(2)}}{\mu_e}\right)^{1/3}} \cdot g\,(M_e, T_e)$$

The integration of equation (3) in each particular case can be avoided for the following two reasons:

Reason 1. Effect of the Reynolds number.

If we assume a law having the form $\mu = kT^{\omega}$ for the viscosity, it may be readily shown [9] that, for pipes which are geometrically similar and which are subjected to identical thermal conditions (this is the case here, since $T_p = T_f$), there is a law of similarity which connects the quantity $\delta^{(1)}/h$ to the Reynolds number $Re_{i,h}$ formed with the generating conditions and the radius h of the throat:

$$\mathcal{R}e_{i,h} = \frac{\rho_i a_i h}{\mu_i}$$

It may be shown that if $C_o = (\delta^{(1)}/h)_o\ Re_{i,h}^{1/6}$ is the initial value at $x = x_o$ /6 of the product $C = (\delta^{(1)}/h)\ Re_{i,h}^{1/6}$, this product may be expressed at the running point x in the following form:

$$(\delta^{(1)}/h)\ \mathcal{R}e_{i,h}^{1/6} = F\,(x/h, x_0/h, C_0, h/R_c)$$

in particular, at the throat (x = 0):

$$(\delta_c^{(1)}/h)\ \mathcal{R}e_{i,h}^{1/6} = F\,(0, x_0/h, C_0, h/R_c).$$

Reason 2: Effect of the Initial Conditions

We have systematically carried out calculations for a series of values for the amount of curvature h/R_c at the throat of the pipe by varying greatly the initial value C_o as well as the abscissa x_o/h of the initial point: provided that the velocity at this point of departure is sufficiently small ($M_o \leq 0.2$), we have found numerically that the value $\delta_c^{(1)}/h \times Re_{i,h}^{1/6}$ at the throat only depends on the amount of curvature h/R_c.

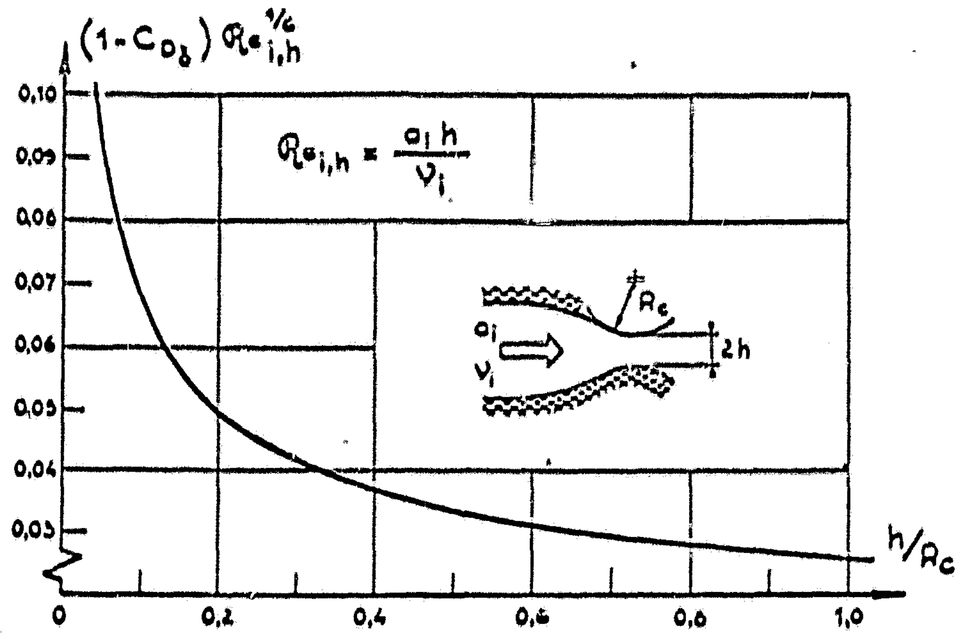

Figure 2.
Calculation of the Flow. Effect of Turbulent Viscosity.

We may then write:

$$(\delta_e^{(1)}/h) \cdot Re_{i,h}^{1/6} = F\,(h/R_c)$$

Having thus calculated the value $F(h/R_c)$ for

$$(0{,}05 \leqslant h/R_c \leqslant 1),$$

and setting

$$C_{D_\delta} = \frac{\text{Flow corrected for the effect of displacement}}{\text{ideal flow } \overline{q}}$$

we immediately obtain the relationship

$$(1 - C_{D_\delta}) \cdot Re_{i,h}^{1/6} = 2\,F\,(h/R_c)$$

Figure 2 gives the variations of this function. /7

For example, if $Re_{i,h} = 10^6$ and $h/R_c = 0.25$, $1 - C_{D_\delta} = 4.5 \times 10^{-3}$.

As a result of calculations which did not take into account the preceding simplifying reasons, the values of C_{D_δ} published by Stratford [6] are in agreement with our results, with the deviation never exceeding $0.5.10^{-3}$ in the region of practical use $0.15 \leq h/R_c \leq 1$.

3. Virial Effect

It frequently happens that the supply pressures of flowmeters reach relatively high levels (> 10 bars). Under these conditions and at moderate generating

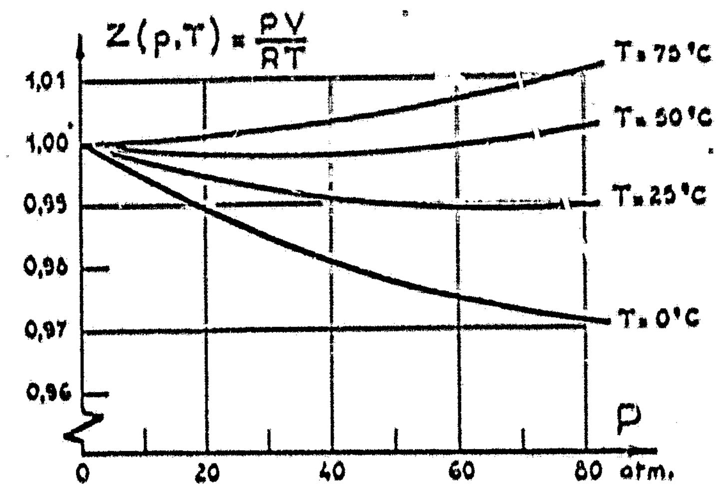

Figure 3. Compressibility Factor Z.

temperatures (between 0 and 50 degrees centigrade), air does not behave like a perfect gas.

Its equation of state therefore takes the following form

$$p = Z(T, \rho) \cdot \rho R T$$

where Z is the compressibility factor which is known and which is determined with the aid of the virial coefficients.

Figure 3, taken from reference [10], gives the variations of Z with p and T.

The tables of Mollier [10] which result from them have made it possible for us to calculate a series of isentropic and monodimensional expansions for different generating conditions and up to M - 1. We have thus determined a coefficient C_{D_v}, the ratio of the real flow with the virial effect to the ideal flow $\overline{q}$ calculated for $\gamma = 1.4$.

Figure 4 gives the calculated values of $(C_{D_v} - 1).10^3$ as a function of p_i and T_i.

It should be noted that the correction is very well respresented, in the /8
generating pressure and temperature regions considered here, by the following practical formula, which is linear as a function of p_i:

$$C_{D_v} = 1 + 0{,}035 \frac{p_i\,(atm)}{T_i\,(^\circ C) + 63}$$

For example, for $p_i = 25$ atm, $T_i = 25^\circ$ C, the virial correction is 1%.

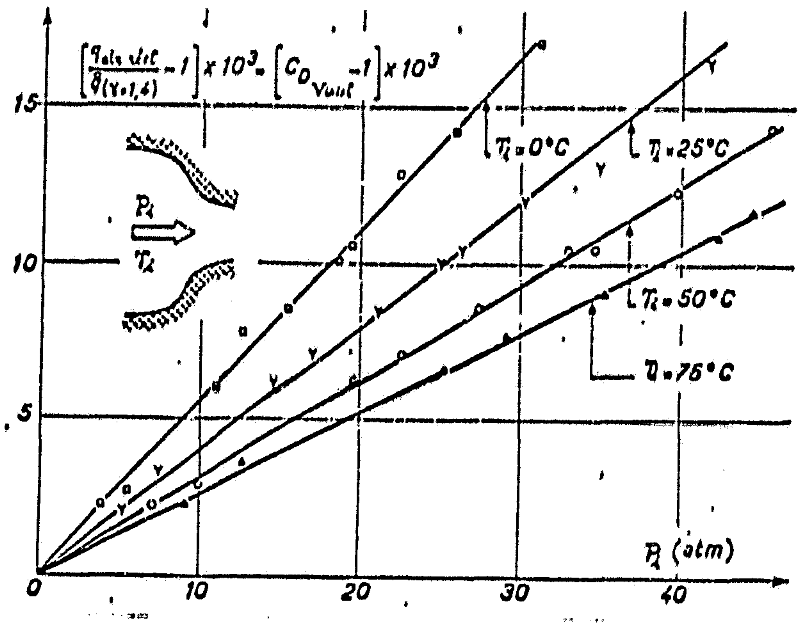

Figure 4. Flow Calculation. Virial Effect.

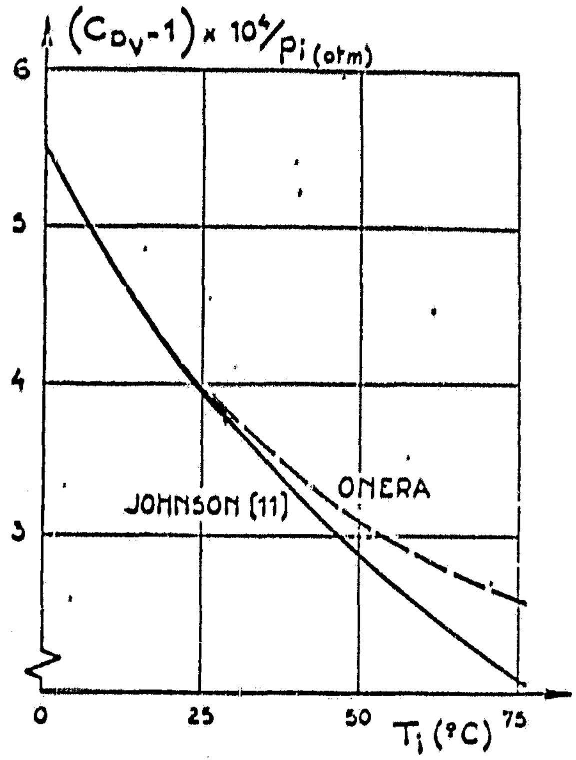

Figure 5. Flow Calculation. Virial Effect. Comparative Results.

Similar calculations have been carried out by Johnson [11] and more /9
recently by J.C. Ascough [12].

In the report by Johnson, we may clearly see the linear character of the correction as a function of the pressure, so that a comparison with our results and those given in reference [11] can be made in the form of Figure 5, where the values of $[C_{D_V} - 1].\frac{10^4}{p_i}$ are given as a function of T_i.

The curves differ slightly above 25° C. This difference must be attributed to the differences existing between the thermodynamic tables utilized in our calculations [10] and those [13] utilized by Johnson. However, at the present time we cannot precisely define the factors which may explain these deviations.

With respect to the results given by Ascough, they are very fragmentary, because the generating pressure does not exceed 10 atm. We obtain from [12], p_i = 10 atm and T_i = 290° C, C_{D_V} = 1.0042. For the same generating conditions, we obtain for our part C_{D_V} = 1.0044. The agreement is therefore very good.

4. Experimental Verification of the Virial Effect

4.1. Introduction

We have just analyzed successively three corrections to be applied to the elementary formula for the flow of a sonic throat expressed by three coefficients:

$$C_{D_K},\ C_{D_\delta},\ C_{D_V}.$$

Each of the corrections obtained is on the order of 1%, and we may therefore write:

$$q_{réel} = C_{D_K} \cdot C_{D_\delta} \cdot C_{D_V} \cdot \bar{q}$$

The recent installation at the Test Center of O.N.E.R.A. at Modane of a new plant for compressed air having increased characteristics (pressure up to 50 bars, flow up to 20 kg/sec) has made it possible to subject the preceding ideas to the test of experimentation, particularly with respect to the effect of the compressibility factor. The principle underlying the experiment consists of determining -- by means of two different methods -- the same output of a constant flow successively traversing two sonic throats, having sufficiently different sections so that the generating pressures upstream from these two throats are of clearly different levels. Therefore, let (Figure 6) two sonic throats (1) and (2) be traversed by the same steady flow.

The flow traversing (1) is:

$$q_1 = k \times \frac{P_{i_1} A_{c_1}}{\sqrt{T_{i_1}}} \cdot C_{D_{K_1}} \cdot C_{D_{\delta_1}} \cdot C_{D_{V_1}}$$

The flow traversing (2) is: /10

$$q_2 = k \times \frac{P_{i_2} A_{c_2}}{\sqrt{T_{i_2}}} \cdot C_{D_{K_2}} \cdot C_{D_{\delta_2}} \cdot C_{D_{V_2}}$$

If the flow is constant: $q_1 = q_2$.

Therefore:

$$\frac{P_{i_1} A_{c_1}}{\sqrt{T_{i_1}}} \cdot C_{D_{K_1}} \cdot C_{D_{\delta_1}} \cdot C_{D_{V_1}} = \frac{P_{i_2} A_{c_2}}{\sqrt{T_{i_2}}} \cdot C_{D_{K_2}} \cdot C_{D_{\delta_2}} \cdot C_{D_{V_2}}$$

or

$$\frac{P_{i_2}}{P_{i_1}} \cdot \frac{A_{c_2}}{A_{c_1}} \cdot \sqrt{\frac{T_{i_1}}{T_{i_2}}} = \frac{C_{D_{K1}}}{C_{D_{K_2}}} \cdot \frac{C_{D_{\delta_1}}}{C_{D_{\delta_2}}} \cdot \frac{C_{D_{V_1}}}{C_{D_{V_2}}}. \qquad (4)$$

Let us consider the right-hand term in the preceding equation (4).

The quantity $\frac{C_{D_{k1}}}{C_{D_{k2}}}$ which is related to the geometry of the two throats is

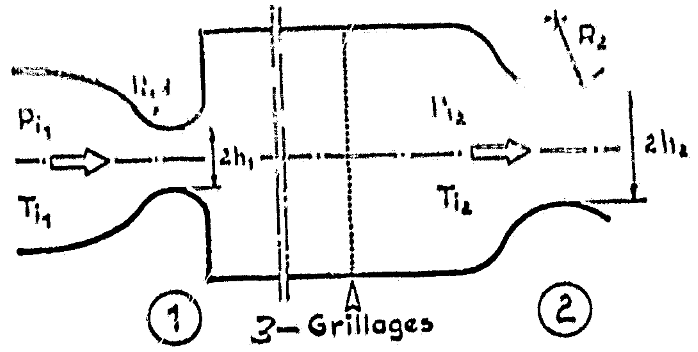

Figure 6. Diagram showing the Principle to be Used in Verifying the Compressibility Effect (Virial Effect) (3) - grating

independent of the generating conditions.

The quantity $\dfrac{C_{D_{\delta_1}}}{C_{D_{\delta_2}}}$ is, in the case under consideration, almost constant, as we shall see further on.

Consequently, the quantity

$$\frac{P_{i_1}}{P_{i_2}} \cdot \frac{A_{c_1}}{A_{c_2}} \cdot \sqrt{\frac{T_{i_1}}{T_{i_2}}}$$

must follow an expansion similar to that of the ratio $\dfrac{C_{D_{v_1}}}{C_{D_{v_2}}}$ when, from one test to the other, one varies the level of the generating pressure P_{i_1}.

This is what the experiments which we are going to describe, and those which were performed at the O.N.E.R.A. Center at Modane were trying to verify.

4.2. Description of the Experimental Arrangement at Modane

The experimental arrangement includes two throats placed in a cascade arrangement and each preceded by a tranquilization chamber. /11

4.2.1. Arrangement upstream from the first throat.

The first throat (Figure 7), with a diameter of 31.981 mm, is preceded by a tranquilization chamber with a diameter of 125 mm. The Mach number M_1 of flow in this chamber is close to 0.04. This tranquilization chamber, which is relatively small, is itself preceded by a spherical buffer of 1 m^3, which provides a connection with the central supply of compressed air. This central supply may furnish in 2 to 5 minutes a flow of air which is essentially constant at a quasi-constant temperature.

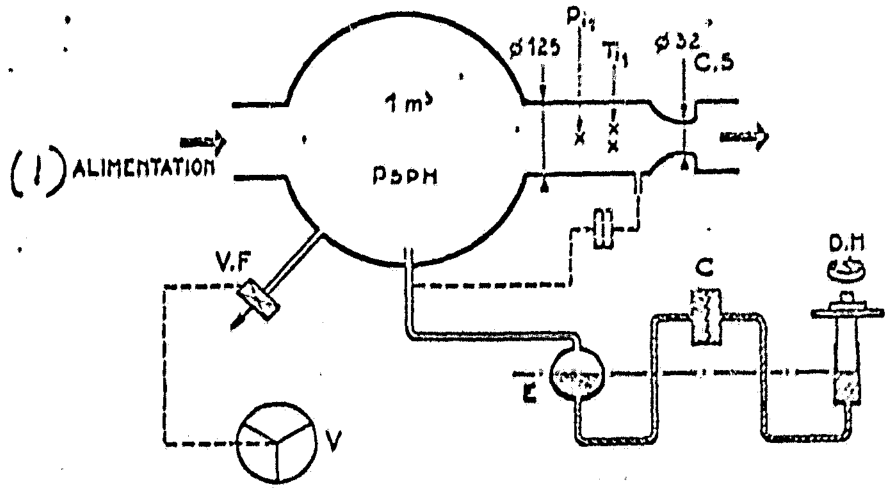

Figure 7. Arrangement Upstream from the First Throat
C.S.: sonic throat upstream
C.: Aqmel capsule
D.H.: Desgranges and Huot manometric balance
E.: air-oil pressure exchanger
V.F.: escape valve
V.: remote control wheel for the escape valve
(1) - supply

An escape valve (V.F.), which is manually controlled by means of a wheel V, makes it possible to provide constant pressure in the sphere P_{sph}.

(A) Measurement of P_{sph}. The pressure of the sphere P_{sph} is transmitted by means of an air-oil pressure exchanger E to a differential Aqmel capsule with gauges C (0-3 bars). The counterpressure is provided by a Desgranges and Huot manometric balance (0-60 bars).

This is the principle underlying the measurement of P_{sph}.

(B) Calculation of P_{i_1}. Calibration before the tests was performed in order to evaluate the coefficient

$$\varepsilon = \frac{P_{sph} - P_{i_1}}{P_{i_1}},$$

for charge losses between the sphere and the input of the first throat (on the order of 1 per thousand).

By knowing P_{sph}, one can also calculate P_{i_1}.

(C) Measurement of T_{i_1}. This is done by means of a thermocouple placed in the flow. /12

4.2.2. Arrangement Upstream from the Second Throat.

The second throat, with variable diameter, is preceded by a tranquilization chamber with a diameter of 170 mm. The Mach number M_2 in this chamber, which varies with the diameter of the throat, always remains very small.

(a) Measurement of P_{i_2}. A method which is identical to that used to measure the pressure in the sphere P_{sph} is used to measure the static pressure p_2 in the tranquilization chamber of the second throat.

A knowledge of M_2 makes it possible to calculate P_{i_2}.

(b) Measurement of T_{i_2}. During one test, the flow upstream from the first throat is maintained at room temperature, so that the thermal exchange with the walls, which is negligible, makes the temperature profile very flat. In the second tranquilization chamber, there is necessarily a temperature deviation between the flow and the walls due to the Joule-Thomson effect. This is the reason why a grating of nine thermocouples is placed in this second chamber, in order to take into account a possible temperature profile. The temperature T_{i_2} is then a weighted average of the nine individual measurements.

4.3. Test Sequence

One test lasts from 1 to 2 minutes depending on the level of the supply pressure P_{sph}, on the order of 10 to 45 bars, with the flow going from 2 kg/sec to 9 kg/sec.

During these gusts, the pressure P_{sph} is kept constant at $\pm$ 5 millibars by means of the escape valve V.F. (See Figure 7), which is controlled manually by the wheel V, depending on the readings of the differential capsule C which are displayed visually by a spot on a luminous screen.

During one gust, the temperature T_{i_1} decreases slightly from 1 to 2 degrees.

All of the quantities are recorded electrically. One gust makes it possible to make about 4 measurement points.

4.4. Experimental Results

Two series of tests were performed corresponding to two different sonic throats downstream, adapted to the second tranquilization chamber. The sonic throat downstream remains unchanged.

The geometric characteristics of the upstream throat and of the two throats downstream are shown in Figure 8. /13

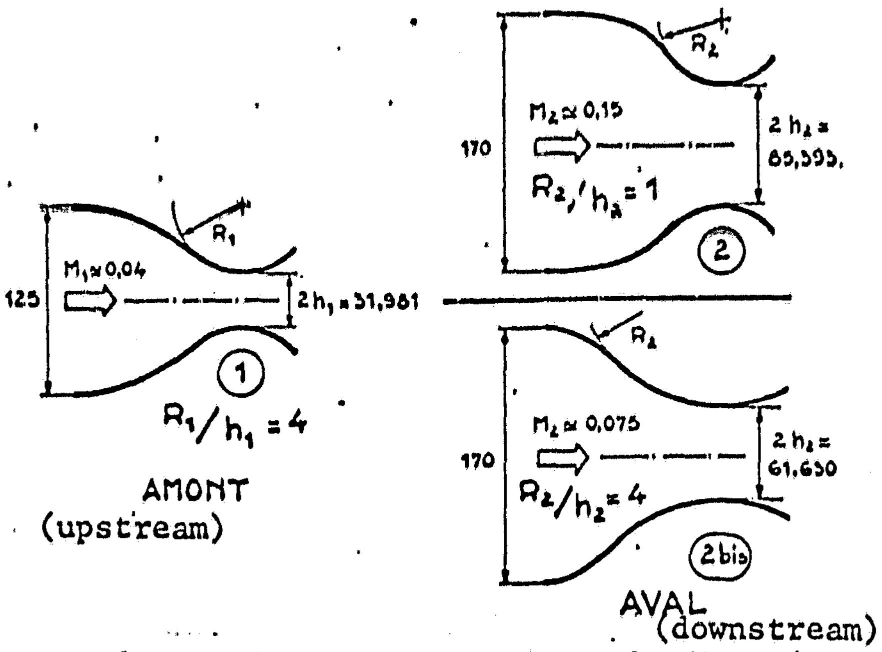

Figure 8. Sonic Throats used in the Experiment

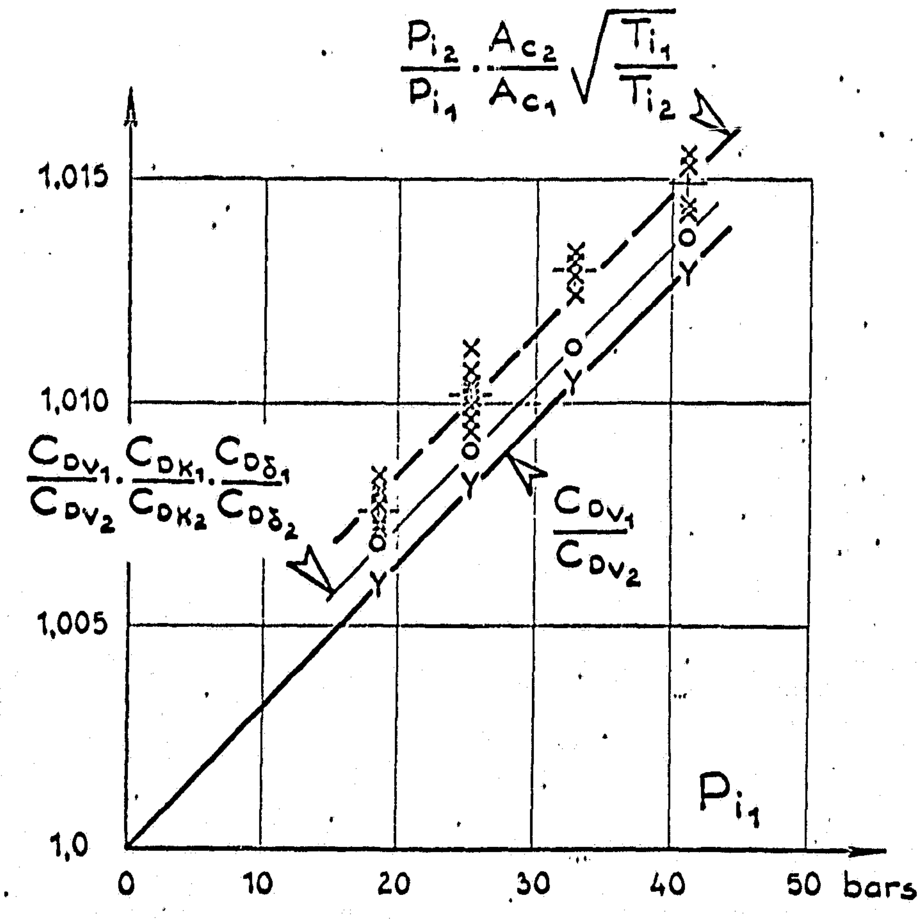

Figure 9. Experimental Results.
Upstream throat (1): $R_1/h_1 = 4$
Downstream throat (2b): $R_2/h_2 = 4$

4.4.1. Experimental Results with the Downstream Sonic Throat No. 2b ($R_2/h_2 = 4$).

These results are shown in Figure 9 where the following are shown as a function of P_{i_1}:

-- the experimental values of the quantity

$$\frac{P_{i_1}}{P_{i_1}} \cdot \frac{A_{c_1}}{A_{c_1}} \sqrt{\frac{T_{i_1}}{T_{i_1}}}$$

corresponding to 5 gusts with different pressure levels, with each gust comprising 4 measurement points (two gusts for $P_{i_1} = 25.3$ bars),

-- the quantity $\frac{C_{D_{v_1}}}{C_{D_{v_2}}}$ calculated from the experimental values of P_{i_1}, P_{i_2}, T_{i1}, T_{i2} by means of the useful relationship given above:

$$C_{Dv} = 1 + 0{,}035 \frac{P_i\,(\text{atm})}{T_i\,(^\circ\text{C}) + 63}$$

-- the quantity $\frac{C_{Dv_1}}{C_{Dv_2}} \cdot \frac{C_{DK_1}}{C_{DK_2}} \cdot \frac{C_{D\delta_1}}{C_{D\delta_2}}$ where $\frac{C_{DK_1}}{C_{DK_2}} = 1$:

The two upstream throats and downstream throats are actually similar geometrically. We thus do not have the uncertainty which occurs in determining the coefficients C_{D_k}.

In addition

$$\left\{\begin{array}{l} C_{D\delta_1} = 1 - 3{,}2 \times 10^{-3} \\ C_{D\delta_2} = 1 - 4 \times 10^{-3} \end{array}\right. \quad \text{for } P_{i_1} = 20 \text{ bars}$$

$$\left\{\begin{array}{l} C_{D\delta_1} = 1 - 2{,}84 \times 10^{-3} \\ C_{D\delta_2} = 1 - 3{,}65 \times 10^{-3} \end{array}\right. \quad \text{for } P_{i_1} = 40 \text{ bars}$$

from which we find that:

$$\left\{\begin{array}{l} \frac{C_{D\delta_1}}{C_{D\delta_2}} = 1 + 0{,}8 \times 10^{-3} \text{ for } P_{i_1} = 20 \text{ bars} \\ \frac{C_{D\delta_1}}{C_{D\delta_2}} = 1 + 0{,}8 \times 10^{-3} \text{ for } P_{i_1} = 40 \text{ bars.} \end{array}\right.$$

First of all, it should be noted that the experimental values are very closely grouped around their average (-|-) within one gust, with the deviation not exceeding 1×10^{-3}. It should also be noted that the experimental values of the quantity

$$\frac{P_{i_1}}{P_{i_2}} \cdot \frac{A_{c_1}}{A_{c_2}} \cdot \sqrt{\frac{T_{i_1}}{T_{i_2}}}$$

increase linearly with P_{i_1} and in a similar manner to the calculated quantity $\frac{C_{D_{v1}}}{C_{D_{v2}}}$, which confirms the effect of the compressibility factor.

It may be finally stated that there is a systematic deviation on the order of 1.2×10^{-3} between

$$\frac{P_{i_1}}{P_{i_2}} \cdot \frac{A_{c_1}}{A_{c_2}} \cdot \sqrt{\frac{T_{i_1}}{T_{i_2}}} \quad \text{and} \quad \frac{C_{Dv_1}}{C_{Dv_2}} \cdot \frac{C_{DK_1}}{C_{DK_2}} \cdot \frac{C_{D\delta_1}}{C_{D\delta_2}}$$

4.4.2. <u>Experimental Results with the Sonic Throat No. 2 ($R_2/h_2 = 1$).</u> /15

These results are shown in Figure 10.

Just as in Figure 9, we obtain the quantities $\frac{P_{i_1}}{P_{i_2}} \cdot \frac{A_{c_1}}{A_{c_2}} \cdot \sqrt{\frac{T_{i_1}}{T_{i_2}}}, \frac{C_{Dv_1}}{C_{Dv_2}}$ (calculated).

$$\text{for } P_{i_1} = 20 \text{ bars} \begin{cases} C_{D\delta_1} = 1 - 3{,}2 \times 10^{-3} \\ C_{D\delta_2} = 1 - 2{,}2 \times 10^{-3} \end{cases}$$

$$\text{for } P_{i_1} = 40 \text{ bars} \begin{cases} C_{D\delta_1} = 1 - 2{,}84 \times 10^{-3} \\ C_{D\delta_2} = 1 - 1{,}95 \times 10^{-3} \end{cases}$$

from which we find that

$$\frac{C_{D\delta_1}}{C_{D\delta_2}} \begin{cases} = 1 - 1 \times 10^{-3} \text{ for } P_{i_1} = 20 \text{ bars} \\ = 1 - 0{,}9 \times 10^{-3} \text{ for } P_{i_1} = 40 \text{ bars.} \end{cases}$$

This calculation enables us to show in Figure 10 the variations of $\frac{C_{Dv_1}}{C_{Dv_2}} \cdot \frac{C_{D\delta_1}}{C_{D\delta_2}}$.

The great degree of uncertainty which appeared above in the determination of the coefficient C_{D_k} for large curvatures prevents us, a priori, from drawing the quantity /16

$$\frac{C_{Dv_1}}{C_{Dv_2}} \cdot \frac{C_{D\delta_1}}{C_{D\delta_2}} \cdot \frac{C_{DK_1}}{C_{DK_2}}.$$

It should first be noted that the experimental values are still better grouped around their average (-|-) and within one gust than in the preceding example, with the deviation not exceeding 0.5×10^{-3} this time.

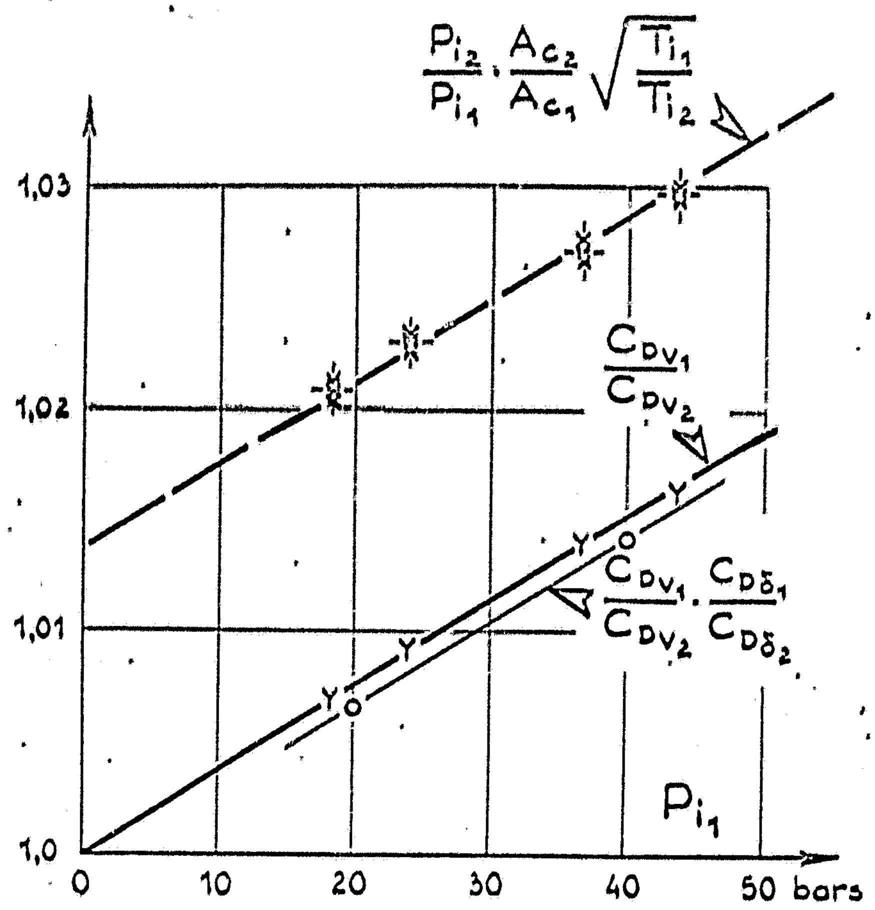

Figure 10. Experimental Results.
Upstream throat (1): $R_1/h_1 = 4$.
Downstream throat 2: $R_2/h_2 = 1$

It should be noted that the quantity $\frac{P_{i_2}}{P_{i_1}} \cdot \frac{A_{c_2}}{A_{c_1}} \cdot \sqrt{\frac{T_{i_1}}{T_{i_2}}}$ increases linearly with P_{i_1}, with the slope equal to that of the quantity $\frac{C_{D_{V1}}}{C_{D_{V2}}}$.

The effect of the compressibility factor is thus again confirmed.

A large divergence should finally be noted

$$\frac{P_{i_2}}{P_{i_1}} \cdot \frac{A_{c_2}}{A_{c_1}} \cdot \sqrt{\frac{T_{i_1}}{T_{i_2}}} \qquad \cdot \qquad \frac{C_{DV_1}}{C_{DV_2}} \cdot \frac{C_{D\delta_1}}{C_{D\delta_2}}$$

This divergence, on the order of 14.5×10^{-3}, is caused in part by the great curvature of the second sonic throat. We shall return to this point in 4.4.3.

4.4.3. Discussion of the Measurement Accuracy

The measurement of pressures P_{i_1} and P_{i_2} by means of the differential Aqmel capsule and the Desgranges and Huot manometric balance yields an absolute error of $\pm 10^{-2}$ bars at the maximum. Therefore,

$$\begin{cases} \dfrac{\Delta P_{i_1}}{P_{i_1}} \simeq 0{,}3 \times 10^{-3} \\ \dfrac{\Delta P_{i_2}}{P_{i_2}} \simeq 1{,}25 \times 10^{-3} \end{cases}$$

The errors involved in the measurement of the diameters of the throats A_{c_1} and A_{c_2} on the order of 2×10^{-3} mm to 5×10^{-3} mm, depending on the diameter, can be neglected.

We assume an error of 0.2° C in the measurement of T_{i_1} (1 thermocouple) and of 0.1° C in the measurement of T_{i_2} (9 thermocouples).

The calculation of the error then shows that the quantity

$$\frac{P_{i_1}}{P_{i_2}} \cdot \frac{A_{c_1}}{A_{c_2}} \cdot \sqrt{\frac{T_{i_1}}{T_{i_2}}}$$

is known with an relative error on the order of 2×10^{-3}. The experimental values obtained show us that around their average the deviation is at the most 1×10^{-3}.

The deviation of 1.2×10^{-3} between

$$\frac{P_{i_1}}{P_{i_2}} \cdot \frac{A_{c_1}}{A_{c_2}} \cdot \sqrt{\frac{T_{i_1}}{T_{i_2}}}, \quad \frac{C_{D_{V_1}}}{C_{D_{V_2}}} \cdot \frac{C_{D_{K_1}}}{C_{D_{K_2}}} \cdot \frac{C_{D_{\delta_1}}}{C_{D_{\delta_2}}},$$

/17

which was found in the first series of tests must be regarded as a systematic error, without knowing to what this error may be attributed.

If we assume that this same systematic error occurs for the second series of measurements ($R_1/h_1 = 4$; $R_2/h_2 = 1$), it must be concluded that the quantity

$\dfrac{C_{D_{k_1}}}{C_{D_{k_2}}}$ has a value of $1 + 13.3 \times 10^{-3}$.

However, the error involved in the determination of $C_{D_{k_1}}$ is negligible since, for small curvatures, all the theories yield identical results: $C_{D_{k_1}} \simeq 1 - 1.4 \times 10^{-3}$.

One can then obtain the value $C_{D_{k_1}}$:

$$C_{D_{K_2}}\,(R_2/h_2 = 1) = 0{,}9853.$$

This value which is shown in Figure 1 has enabled us to draw the curve D tangent to the curve B for $h/R_c \_ 0.4$ and passing through the experimental point: $h/R_c = 1$, $C_{D_k} = 0.9853$

General Conclusion

We have just successively analyzed three corrections to be applied to the elementary formula for the flow of a sonic throat expressed by three coefficients:

$$C_{D_K}, \quad C_{D_\delta}, \quad C_{D_V}$$

Each of the corrections obtained is on the order of 1%, and we can therefore write:

$$q_{réel} = C_{D_K} \cdot C_{D_\delta} \cdot C_{D_V} \cdot \bar{q}.$$

The diagrams represented here apply to air. The coefficient C_{D_δ} is only given here in the case of a turbulent boundary layer in the presence of an adiabatic wall. The accuracy measurements, performed at Modane, confirm the calculation of the compressibility effect.

In the flow measurements it is wise to avoid the high curvatures at the level of the throat, especially because -- in agreement with Stratford -- we estimate that a moderate curvature (R/h = 4) makes it possible to reduce to a minimum the possible error on the effect of flow reduction caused by the boundary layer, whose laminar character or turbulent character cannot always be affirmed a priori.

References

1. P. Carriere. Calculation of the Supersonic Flow of Real Gas by the Method of Characteristics. Ecole Nationale Superieure de l' Aeronautique, 1964.

2. M. Fenain. Investigation of the approximations of the equations governing the gas flow. Application to plane pipes. Rech. Aer. No. 33, 1953.

3. D. Guiraud-Vallee and M. Fenain. An example of the numerical calculation of a plane, subsonic-supersonic flow. Internal Technical Report of O.N.E.R.A. (November, 1967).

4. I.M. Hall. Transsonic flow in two-dimensional and axially symmetric nozzles. Mechanics of Fluids Department, Manchester University, 1962.

5. M.V. Herbert and D.L. Martlew. The design point performance of model internal - Expansion propelling nozzles with area ratios up to 4. N.G. T.E. Report No. 258 (December, 1963).

6. B.S. Stratford. The calculation of the discharge coefficient of profiled choked nozzles and the optimum profile for absolute air flow measurement. Jl. R. Aeronaut. Soc., 4, 1964.

7. D. Masure. Viscosity effects and virial effects upon the measurement of flow by the sonic throat. Rech. Aer. No. 120, 1967.

8. R. Michel. Turbulent boundary layers and practical calculation of the boundary layers in a compressible fluid. Cours a l'Ecole Nationale Superieure de l'Aeronautique, 1963.

9. P. Carriere. Viscous effects on propulsion nozzles (short course on internal aerodynamics of rocket engines). Von Karman Institute for Fluid Dynamics, Rhode-Saint-Genese (April 21, 1966).

10. A. Michels, T. Wassenaar and G.J. Wolkers. Thermodynamical properties of air for temperatures between +75° C and -170° C and pressures up to 1200 atm. App. Sc. Res. Section A, vol. 5, 1955, p. 121 to 136.

11. Johnson, R.C. Real-Gas effects in critical - flow- through nozzles and tabulated thermodynamic properties. Lewis Research Center, Cleveland, Ohio, N.A.S.A. TN-D-2563 (January, 1965).

12. J.C. Ascough. Real Air effects in propelling nozzles. N.G.T.E. Report No. R. 285 (September, 1966).

13. Hilsenrath, Joseph, et al. Tables of thermodynamic and transport properties of air, argon, carbon dioxide, carbon monoxide, hydrogen, nitrogen, oxygen, and steam. Pergamon Press, 1960.